Eur. Phys. J. A (2025) 61:4
https://doi.org/10.1140/epja/s10050-024-01462-9

THE EUROPEAN PHYSICAL JOURNAL A

Regular Article - Experimental Physics

Direct measurement of the ^{19}F(p,α)^{16}O reaction using the LHASA detector array

T. Petruse[1,2,a], G. L. Guardo[3], D. Lattuada[3,4], M. La Cognata[3], D. L. Balabanski[1,2], E. Aciksoz[1], L. Acosta[6], L. Capponi[1], D. Carbone[3], S. Cherubini[3,5], D. Choudhury[1], G. D'Agata[5,7], A. Di Pietro[3], P. Figuera[3], M. Gulino[3,4], A. I. Kilik[7], M. La Commara[8], L. Lamia[3,5,12], C. Matei[1], S. Palmerini[9,10], R. G. Pizzone[3,5], S. Romano[3,4,12], P.-A. Söderström[1], R. Sparta[3,4], A. Tumino[3,4], S. Viñals[11]

[1] Extreme Light Infrastructure Nuclear Physics/IFIN-HH, Magurele, Romania
[2] Scoala Doctorala de Ingineria si Aplicatiile Laserilor si Acceleratorilor, Universitatea Politehnica, Bucuresti, Romania
[3] Laboratori Nazionali del Sud INFN, Catania, Italy
[4] Universita di Enna "Kore", Enna, Italy
[5] Dipartimento di Fisica e Astronomia "E. Majorana", Universita degli Studi di Catania, Catania, Italy
[6] National Autonomous University of Mexico, Mexico D.F., Mexico
[7] Nuclear Physics Institute of ASCR, Rez, Czech Republic
[8] Dipartimento di Pharmacy, Universita di Napoli Federico II, Naples, Italy
[9] Dipartimento di Fisica Universita di Perugia, Perugia, Italy
[10] INFN Sezione di Perugia, Perugia, Italy
[11] Instituto de Estructura de la Materia, CSIC, Madrid, Spain
[12] Centro Siciliano di Fisica Nucleare e Struttura della Materia (CSFNSM), Catania, Italy

Received: 28 May 2024 / Accepted: 25 November 2024

Communicated by Anu Kankainen

Abstract The low-energy ^{19}F(p,α)^{16}O reaction has significant implications for nuclear astrophysics. The ^{19}F(p, α)^{16}O reaction occurs via three channels: (p,α_0), (p,α_π), and (p,α_γ). At lower temperatures, below 0.15 GK, the (p,α_0) channel is the dominant contributor of the reaction. The ^{19}F(p,α_0)^{16}O reaction cross section in the energy range of 400–900 keV was studied in this work. Recent data in the literature reveals a roughly 1.4 increase compared to prior findings reported in the NACRE (Nuclear Astrophysics Compilation of REactions) compilation. Therefore, we present new additional result of the study published in EPJA [22] employing a silicon strip detector array (LHASA - Large High-resolution Array of Silicon for Astrophysics). The anguar distributions, the reaction cross sections and the astrophysical *S-factors* of the (p,α_0) channel were obtained through this experiment. Our findings resolve the discrepancies that exist between the two previously available data sets in the literature.

1 Astrophysical motivation and state of the art

The low-energy ^{19}F(p,α)^{16}O reaction serves as a crucial intersection point between the CNO and NeNa cycles in stars, competing with the ^{19}F(p,γ)^{20}Ne reaction [33,34]. Moreover, it plays a critical role in hydrogen-rich stellar environments as the main fluorine destruction channel, and it may also contribute to nucleosynthesis in hydrogen-deficient post-Asymptotic Giant Branch (AGB) stars [35,36]. However, theoretical models currently predict higher fluorine abundances in AGB stars than observed [37], which necessitates further investigation of reactions involving fluorine.

The origin of Galactic Fluorine is a topic of ongoing debate in modern astrophysics. As fluorine is highly sensitive to the physical conditions within stars, it is often used to probe nucleosynthesis scenarios [1]. However, its nucleosynthetic origin is the least understood of all light elements [2]. Stellar model calculations and observational data have suggested several possible sites for the production of ^{19}F [1,3]. ^{19}F production in type II core-collapse supernovae (SNe) by neutrino spallation on ^{20}Ne has been also proposed [4]. ^{19}F overabundances (with respect to solar) were observed in red giant stars by Jorissen et al. [5], who provided evidence for ^{19}F production during shell He burning in AGB stars [6,7]. He burning in Wolf-Rayet stars was identified by Meynet and Arnould [8]. In addition, Kobayashi et al. [9] considered neutrino-process nucleosynthesis as the primary origin of ^{19}F in metal-deficient stars (Type II and Ia supernovae and hypernovae) and AGB stars. The question of how each candidate

[a] e-mail: teodora.petruse@eli-np.ro (corresponding author)

Published online: 15 January 2025

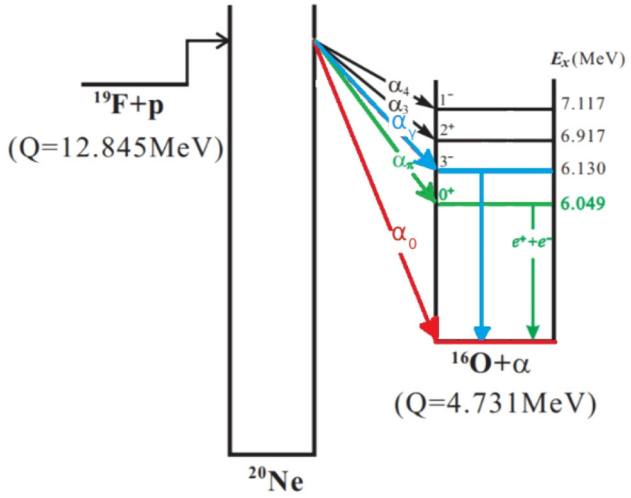

Fig. 1 ^{19}F + p interaction, by forming the compound nucleus ^{20}Ne, which will break into ^{16}O and ^{4}He. The α_0 reaction channel to the ^{16}O ground state is shown in red, the α_π reaction channel to the ^{16}O first excited state is shown in green and the α_γ reaction channel to the ^{16}O second excited state is shown in blue

site contributes to solar-system and galactic fluorine remains open, and the knoledge of the precise rate of the ^{19}F(p,α)^{16}O reaction is essential in finding the answer.

AGB stars have long been considered the primary source of galactic fluorine [5]. However, observed fluorine over-abundances cannot be explained by current AGB models alone, suggesting the involvement of additional mixing effects. It is believed that fluorine is produced in the He-rich intershell and transported to the surface through recurrent dredge-up episodes [10]. Recent work by Palmerini et al. [11,31,32] examined the impact of extra mixing and different rates of the ^{19}F(p,α)^{16}O reaction on the surface abundance of fluorine in AGB stars. Firstly they found that the models can not account for the observed F abundances. By varying the reaction rate by a factor of two led to a 50% variation of the abundance of ^{19}F in the He intershell (inner stellar layer). In the stellar surface the difference in the abundances are smaller. The ^{19}F(p,α)^{16}O reaction occurs via three channels: (p,α_0), (p,α_π), and (p,α_γ) (Fig. 1). At low temperatures around 0.05 GK, the (p,α_π) channel contributes less than 10%, while the (p,α_γ) channel dominates at temperatures above 0.2 GK. At temperatures around 0.15 GK, the (p,α_0) channel is the dominant contributor (Fig. 2) [12,13].

The ^{19}F(p,α)^{16}O reaction is crucial for understanding the nucleosynthesis of fluorine in astrophysical environments. However, the *S-factors* and branching ratios for the reaction's outgoing channels are still uncertain at astrophysical energies, highlighting the need for better measurements [13]. In the past, the Nuclear Astrophysics Compilation of Reaction Rates (NACRE) extrapolated the S-factor from direct data available in the literature in the $E_{CM} = 0.46 - 2.54$

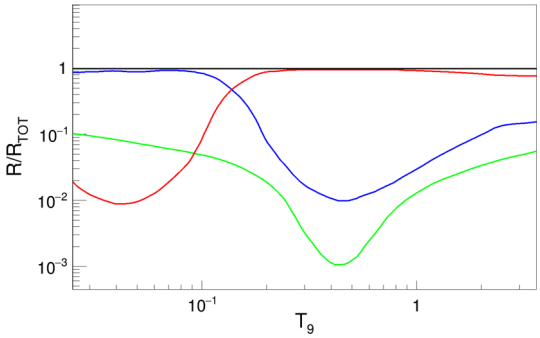

Fig. 2 The contribution of each channel to the total reaction rate. The total reaction rate, normalized to unity is shown in black. The contribution of ^{19}F(p,α_0)^{16}O to the total reaction rate is shown in red, the contribution of ^{19}F(p,α_π)^{16}O to the total reaction rate is shown in green, and the contribution of ^{19}F(p,α_γ)^{16}O to the total reaction rate is shown in blue

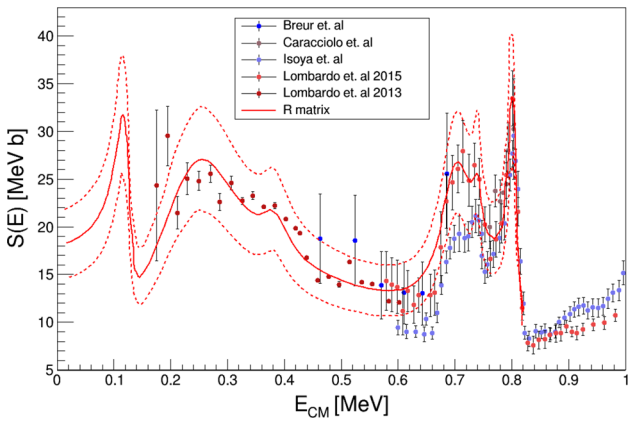

Fig. 3 S-factor of the ^{19}F(p,α_0)^{16}O reaction available in literature (see text for details). Figure from [22]

MeV energy domain [15]. Recently, two experimental studies have been reported: the first one is a direct measurement in the energy range $E_{CM} = 0.2-1$ MeV [16], and the second one uses the Trojan Horse Method (THM) to explore the low energy region [12,17,30]. The latter technique allowed the authors to excite several states of ^{20}Ne, leading to a significant increase in the reaction rate at astrophysical energies. A summary of the S-factors from available literature data for the ^{19}F(p,α)^{16}O reaction is shown in Fig. 3, indicating a large discrepancy between the most recent data and the previous ones in the peaks centered at 681 and 738 keV in the center of mass system [12,16,18–22].

In the present paper, we offer a complete and comprehensive report of the ^{19}F(p,α_0)^{16}O reaction, discussed in the previous paper of Guardo et al. [22]. Our study focuses on the energy range of $E_{CM} = 400 - 900$ keV, and we have derived the astrophysical *S-factors* based on the measurement reported in the present article. This paper discusses the experimental details such as beam, target and detection setup. It also describes how the angular distribution are deduced and

integrated in order to extract the reaction cross section and *S-factor*.

2 Experimental details

The experiment was performed at INFN Laboratori Nazionali del Sud, Catania (Italy), using the 15 MV Tandem Van de Graaff accelerator to produce a ^{19} F beam with an energy range of 9.0 to 18.5 MeV and a 1 mm diameter spot size on the target. Thin self-supported polyethylene targets (CH_2) of approximately 100 μg/cm^2 were placed at a 90° angle with respect to the beam direction and changed frequently (every 5–6 h) to avoid degradation. The detection setup, illustrated in Fig. 4, consisted of six annular single sided silicon strip detectors that were mounted in a lamp-shade configuration to form the Large High-resolution Array of Silicon for Astrophysic (LHASA). LHASA was optimized to detect α particles in a wide angular range (from 10° to 32°) and was positioned 10 cm from the target. To suppress strong fluorine and carbon scattering, a 15 μm thick aluminum shield was placed in front of the LHASA detector array, introducing a threshold of 4 MeV in α detection and an energy straggling of less than 2%. However, this did not pose a problem for the experiment as detailed kinematical calculations showed that α particles originating from the proton-fluorine interaction were expected with a minimum energy of 7 MeV. The trigger of the data acquisition was the total OR of all the strips from the detectors. The signals processed using charge preamplifiers, programmable amplifiers and analog to digital converters (ADCs) were read by an acquisition system for online visualization and data storage for offline analysis.

2.1 Beam and target

The beam energy, target thickness, charge state of the beam and the beam time used for each energy are shown in Table 1, while the center of mass energy is available in Table 2. The center of mass energy is calculated considering that the reaction takes place in the center of the target.

During the experiment, we employed an on-line monitoring system for the target. A tightly collimated detector with an area of 3 mm^2 was placed at 45° with respect to the beam direction to detect forward recoiling protons. To calibrate the monitor detector, a standard ^{241}Am-^{239}Pu-^{244}Cm α-source, was positioned in front of it at a distance of 70 cm, within the vacuum chamber. In Fig. 5, a spectrum obtained with this silicon detector at 15 MeV ^{19}F beam on $C H_2$ target is shown. The first peak represents the protons coming from ^{19}F+p elastic scattering, and the second peak represents the carbon from ^{19}F+^{12}C elastic scattering.

To measure the beam current, we utilized a Faraday cup placed downstream of the target and reduced secondary electron effects by applying a suppression voltage of – 300 V. The reaction chamber was maintained under high vacuum conditions, with a pressure better than 2 x 10^{-6} mbar.

We used the on-line visualization of the monitor detector spectra to supervise the degradation of the target. The degradation of the target is mainly due to sputtering effects of

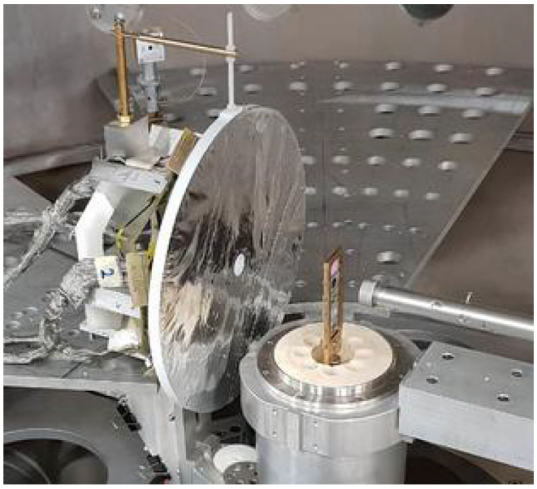

Fig. 4 LHASA - the experimental set-up used for the study of ^{19}F(p,α)^{16}O reaction cross section. The beam is coming from the right side of the picture. The target is placed in the target ladder shown in the middle of the picture and the detection system is shown in the left part of the picture. The detectors were shielded with 15 μm thick aluminum foil

Table 1 Beam and target details

E (MeV)	E_{loss} (MeV)	Target ($\mu g/cm^2$)	Charge state	Time (h)
9.0	0.84	120	3	48
13.0	0.84	115	3	36
14.0	0.36	50	3	24
14.5	1.22	120	3	24
15.0	0.84	100	3	36
16.0	0.74	105	4	18
18.5	0.58	80	4	18

Table 2 Center of mass energy

E (MeV)	Center of mass energy (keV)
9.0	408
13.0	608
14.0	682
14.5	689
15.0	708
16.0	763
18.5	896

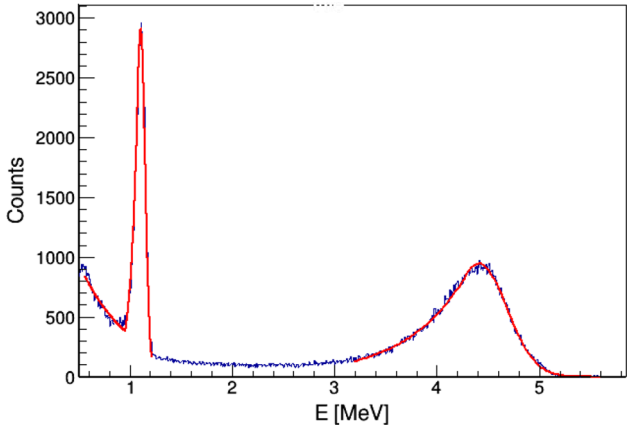

Fig. 5 Monitor detector spectrum obtained at 15 MeV ^{19}F beam on CH_2 target. The first peak represents the protons coming from ^{19}F+p elastic scattering, and the second peak represents the carbon from ^{19}F+^{12}C elastic scattering

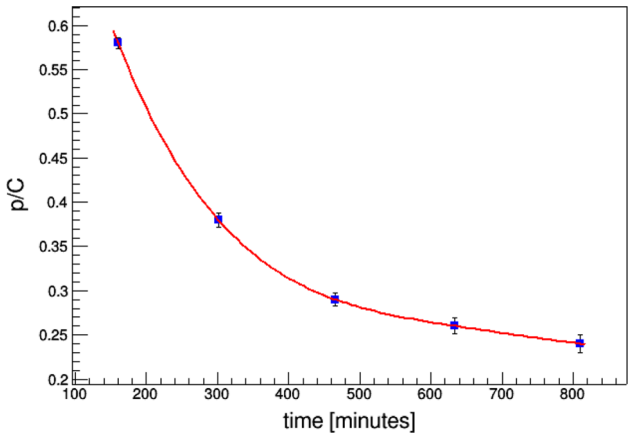

Fig. 6 Target degradation - proton to carbon ratio over time. Figure taken from Ref. [22]

thermal evaporation [38]. Specifically, we checked the proton to carbon ratio as a function of time. As shown in Fig. 6, the target needed to be changed every 6–7 h.

The monitor detector was used also for the normalization procedure. By knowing the ^{19}F + p elastic cross section [20], the solid angle of the monitor detector ($\Delta\Omega_m$) and the measured number of recoiled protons ($N_{protons}$) coming from ^{19}F beam on CH_2 target, the following value was extracted:

$$n = N_{beam}N_{target} = \frac{N_{protons}}{\sigma_{Ruth}\Delta\Omega_m} \quad (1)$$

This value was further used for calculating the cross section of interest, taking into account the detected number of particles and the solid angle of each strip in the array (N_α and $\Delta\Omega_s$):

$$\sigma = \frac{N_\alpha}{n\Delta\Omega_s} = \frac{N_\alpha}{N_{protons}}\frac{\Delta\Omega_m}{\Delta\Omega_s}\sigma_{Ruth} \quad (2)$$

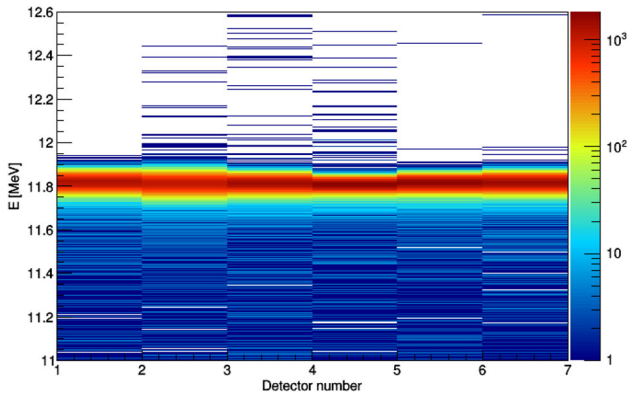

Fig. 7 12 MeV ^6Li beam on ^{12}C target, each bin represents the same strip from all 6 detectors

The error of this procedure will depend on the uncertainty in the solid angles of monitor and strips and marginally the statistics.

2.2 Set-up

The YY1 silicon-strip detector from Micron Semiconductor [23] is a circular sector detector consisting of 16 front strips, 3 mm in width each, with an inner diameter of the active area of 100.0 mm and an outer diameter of the active area of 259.8 mm. Running at a full depletion bias of 90 V, this 300 μm thick detector has a resolution better than 1% for 5.5 MeV α particles. For this experiment, the LHASA detector array consisted of 6 YY1 silicon strip detectors arranged in a lamp-shade configuration. It had 96 channels of associated electronics and it was chosen due to its angular coverage (10° to 32°) and good energy resolution. Each of YY1 detector of the LHASA setup was oriented at 46.1° relative to the beam direction. Solid angles were determined using the simulations, to an accuracy of better than 0.5%. Each bin from Fig. 7 represents the elastic scattering of 12 MeV ^6Li beam on ^{12}C target. From Fig. 7 it is clear that the detectors were aligned between themselves.

The system was fixed inside the vacuum chamber with high-precision screws, with the center of the array aligned with the beam line. Figure 8 shows a drawing of the setup. This alignment is crucial, as it ensures knowledge of the angle with respect to the target for each strip at a given target-detector distance.

3 Data analysis

3.1 Calibration procedure and simulations

To calibrate the detector in energy, we conducted ^{6}Li elastic and inelastic scattering irradiation in the energy range of 12–

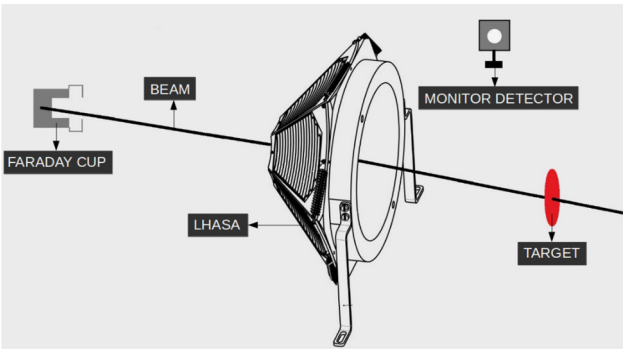

Fig. 8 LHASA drawing of the the experimental set-up used for the study of ^{19}F(p,α)^{16}O reaction cross section. The beam is coming from the right side of the image. The target is shown as a red disk in the right part of the image and the the detection system is shown in the middle of the image. The Faraday cup was placed behind the detection system and it is shown in the left part of the image. The monitor detector was placed at 45° with respect to beam direction and it is shown in the upper part of the image

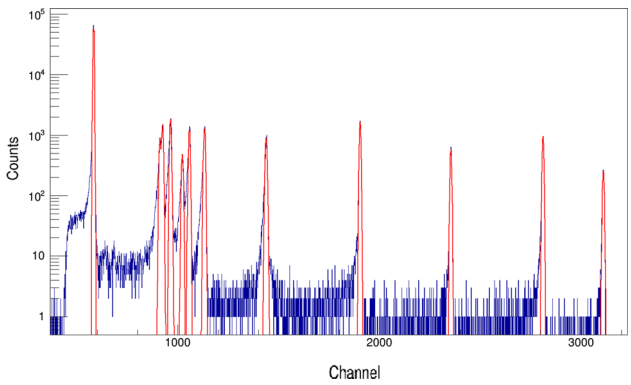

Fig. 9 Energy calibration of YY1 detectors. The peaks are coming from ^{6}Li elastic and inelastic scattering in the energy range 12–20 MeV through the interaction with a gold and carbon target and from a ^{228}Th α-source

20 MeV. These experiments involved interactions with a gold and carbon target, as well as the use of a ^{228}Th α-source. Figure 9 displays all of the peaks observed during calibration procedure.

To accurately associate the observed peaks with their corresponding energy values, it was necessary to account for the energy lost by particles inside the target and in the dead layer of the detectors. This was achieved by utilizing simulation codes for two-body reactions, which considered the energy loss of both the incoming and outgoing particles. The emission angles were also taken into account, as different detection angles result in varying path lengths and energy losses for each particle. We employed the LISE++ [24] software to perform these calculations.

To verify the quality of the calibration, we conducted independent simulations using the open-source Monte Carlo (MC) simulation GROOT [25], which is based on GEANT4

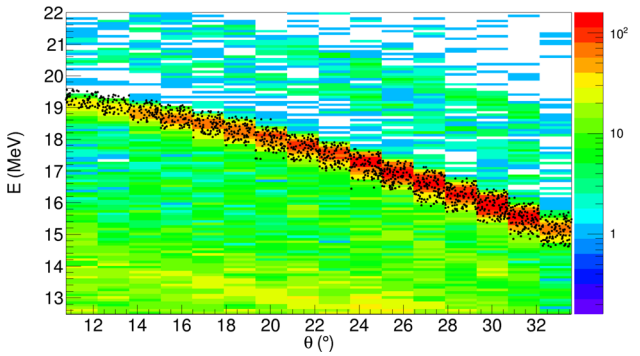

Fig. 10 Agreement between the simulated data (reported with black dots) and the calibrated experimental points for a beam energy of 18.5 MeV

tracking libraries and the n-body event generator of ROOT. Figure 10 illustrates the excellent agreement between the simulated and calibrated experimental data for the ^{19}F(p,α_0)^{16}O channel. This confirms the reliability of the detector calibration. GROOT also allowed us to import CAD files of the detector geometry, which enabled us to evaluate the circular symmetry of the mounted LHASA setup. Our analysis revealed a shift from the symmetrical position less than 5 mm.

In order to account for the lamp-shade configuration of LHASA detector, the experimental data was scaled to a spherical configuration. The average angle and the solid angle associated with it was obtained using GROOT MC simulation environment.

3.2 Angular distributions

After selecting the $^{19}F(p,\alpha_0)^{16}O$ channel and verifying the coherence of the geometrical placement of the LHASA detector, we extracted the experimental angular distributions and compared them with theoretical calculations for each energy. Our results exhibit slopes that are consistent with those reported in Ref. [16]. The primary difference arises from the symmetry of our angular distributions, which experimentally cover only forward angles, leading us to assume that the angular distributions are symmetric with respect to 90°. We anticipate that a stronger forward-backward asymmetry of the angular distribution would be evident in the non-resonant region or in the area with overlapping resonances. This phenomenon may be attributed to interference effects between opposite parity close-lying resonances [12]. The red points from Fig. 12 represent the experimental data, while the black and green lines are the theoretical Legendre polynomials. The green line represents the Legendre polynomial taken from Ref. [16] and it was used as a comparison of our result with the already published data in the literature. Figure 12 demonstrate that our findings are in good agreement with

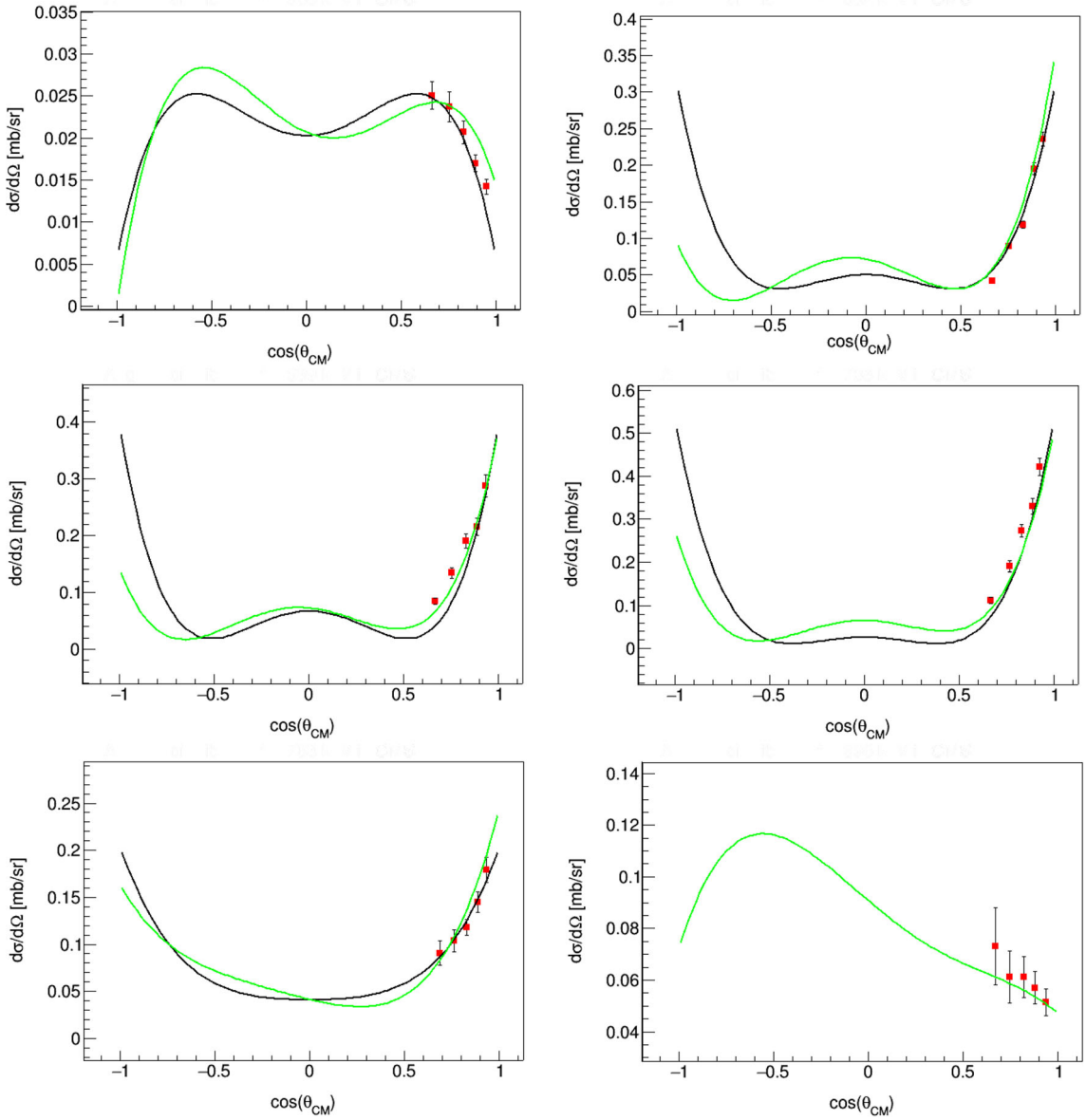

Fig. 11 Red dots represent experimental points, while and black line represents the Legendre polynomial with the best fit to experimental data for the following E_{CM}: **a** 608 keV; **b** 682 keV; **c** 689 keV; **d** 708 keV; **e** 763 keV and **f** 896 keV. Uncertainty in the energy values where evaluated at a maximum of 5 keV The green line represents the Legendre polynomial used by Ref [16]

Table 3 Legendre polynomials coefficients

E_{CM} (keV)	A_0	A_1	A_2	A_3	A_4
608	0.02105±0.00526	0.0	-0.00627±0.00015	0.0	-0.01052±0.00262
682	0.07024±0.00562	0.0	0.13085±0.01047	0.0	0.09818±0.00785
689	0.08122±0.00649	0.0	0.15182±0.01214	0.0	0.15069±0.01205
708	0.09635±0.00674	0.0	0.25984±0.01751	0.0	0.15433±0.01080
763	0.07996±0.00752	0.0	0.09878±0.00942	0.0	0.02895±0.00241
896	0.08603	-0.03239	-0.01721	0.01984	-0.01053

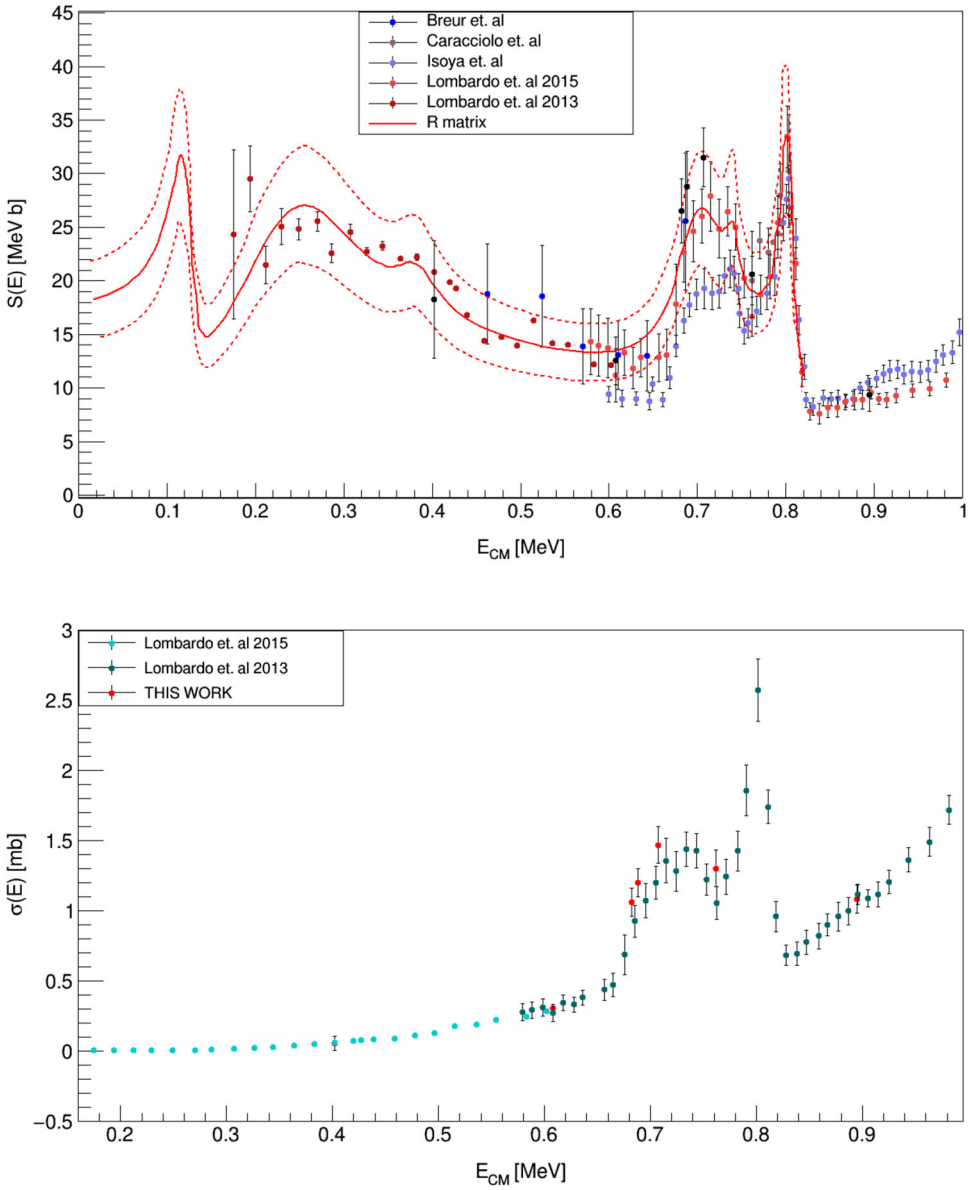

Fig. 12 **a** Astrophysical S(E)-factor for the $^{19}F(p,\alpha_0)^{16}O$ reaction measured in the present experiment (full black points) compared with the available data in the literature, taken from Ref. [22]; **b** Cross section for the $^{19}F(p,\alpha_0)^{16}O$ reaction measured in the present experiment (full red points) compared with Ref. [16] and Ref. [21]

previous data from the literature [16], with discrepancies of approximately 5% between our measurement and the data in Ref. [16] for plots (a), (b), (c), (d), (e). For plot (f) we could not assume symmetry of the angular distributions, so the the experimental points were overlapped with the Legendre polynomial found in Ref [16].

Our spin and parity assignments for all measured energies agree with existing data in the literature. To obtain the total cross section, σ(E), angular distributions were integrated over 4π. For energies outside the range explored in this experiment, we assumed the angular distribution trend to be the best-fit to experimental angular distributions in terms of 4^{th} order Legendre polynomials. At these low energies, only p and d partial waves are expected to contribute. The coefficients of the Legendre polynomials are presented in Table 3.

After the ^{19}F beam interacts with the protons from the CH_2 target, ^{20}Ne is formed in excited state. The increase of the A4 term in the energy range of 0.65−0.75 MeV can be attributed to the excitation of the broad 2+ state in ^{20}Ne. Similarly, the increase of the A2 term in the same energy range can be attributed to the excitation of the broad 1- state in ^{20}Ne.

4 Results

Figure 13 shows (a) the *S-factor* of the $^{19}F(p,\alpha_0)^{16}O$ reaction, already published in Ref. [22] and (b) the cross section of the $^{19}F(p,\alpha_0)^{16}O$ reaction. In the upper part (a) of Figure 13 it is shown the data taken from our work presented by black closed circles, and previous measurements presented

as follows: red continuous line represents the data of Ref. [12], blue closed circles the data of Ref. [18], light brown closed circles the data of Ref. [20], light blue closed circles show the data of Ref. [19], light red closed circles represents the data of Ref. [16] and red closed circles show the data of Ref. [21]. In the lower part of Figure 13 (b) it is shown the data taken from our work presented by red closed circles, and previous measurements presented as follows: light blue closed circles represents the data of Ref. [21] and blue closed circles show the data of Ref. [16].

The error bars of the present data take into account statistical errors, overall systematic errors (including energy calibration and angular integration errors), and uncertainties due to beam and target particle measurement. The number of particles in the beam and target was calculated using the elastic cross section, measured by the monitor detector which was recording the forward scattered protons and carbons from the target. The total error of this measurement accounts for 0.5% for the center of mass energy, while the horizontal bars address the total error of 7–8%. The overall cross section error comes from the statistical and systematical error.

5 Conclusions

In an attempt to solve the discrepancy between the new available data in the ^{19}F(p,α)^{16}O literature and the previous data reported in the NACRE compilation, for the ^{19}F(p,α)^{16}O reaction cross section, the new measurements we already discussed in Ref [22] is in-deep discussed here. This measurement has the aim of reducing the uncertainties in the nuclear reaction rates in the energy region from 0.4 MeV up to 0.9 MeV in the center-of-mass system. The results are in agreement with previous assignments of spin-parity of the resonances situated at 681 and 738 keV in the center-of-mass system, which is due to the population of the 13.529 and 13.586 MeV excited levels of ^{20}Ne. Moreover, the resulting cross section confirms the previous data of Lombardo et al. [16] and Breuer et al. [18], solving the discrepancy between the latest measurements and the previous data reported in the NACRE compilation in the energy region of interest(0.4−0.9 MeV), with potential consequences for the astrophysical reaction rate and stellar models calculations.

The ^{19}F(p,α)^{16}O reaction occurs via three channels: (p, α_0), (p, α_γ), (p, α_π). The (p, α_π) channel provides less than 10% contribution at low temperatures approximately 0.05 GK; the (p, α_γ) channel dominates at temperatures above 0.2 GK. Despite its importance, the S-factors of the (p, α_π) and (p, α_γ) outgoing channels in the ^{19}F(p,α)^{16}O reaction are still largely uncertain at astrophysical energies, pointing out the need for better measurements. This experiment gives us confidence to propose a new experimental campaign aimed at measuring a wider angular range (adding LHASA with the Extreme Light Infrastructure - Nuclear Physics Sillicon Strip Array (ELISSA) detector [26]) and a lower energy range. In addition, the good identification of the channel confirmed by our simulation code strongly push for a measurement focused on the critical ^{19}F(p,α_π)^{16}O and ^{19}F(p,α_γ)^{16}O channel reactions [27–29].

Acknowledgements This work is partially supported by the Extreme Light Infrastructure Nuclear Physics Phase II, a project cofinanced by the Romanian Government and the European Union through the European Regional Development Fund - the Competitiveness Operational Programm (1/07.07.16, COP, ID1334), by ENSAR2, a project financed by the European Union's Horizon 2020 research and innovation programm under grant agreement No. 654002, by the Italian Ministry of University (MIUR) under grant LNS - Astrofisica Nucleare (fondi premiali) and under the contract PN 23 21 01 06 sponsored by the Romanian Ministry of Research, Innovation and Digital- ization, by MEYS Czech Republic under the project EF16- 013/0001679, and by DGAPA-PAPIIT IG101423 project.

Data Availability Statement Data will be made available on reasonable request. [Author's comment: All data generated during this study are contained in this published article.]

Code Availability Statement This manuscript has no associated code/software. [Author's comment: No particular code was used for data analysis.]

References

1. S. Lucatello, T. Masseron, J.A. Johnson et al., Astrophys. J. **729**, 40 (2011)
2. D. Clayton, *Handbook of Isotopes in the Cosmos: Hydrogen to Gallium*, 1st edn. (Cambridge University Press, Cambridge, 2003)
3. A. Renda, Y. Fenner, B.K. Gibson et al., Mon. Not. R. Astron. Soc. **354**, 575 (2004)
4. S.E. Woosley, W.C. Haxton, Nature (London) **334**, 45 (1988)
5. A. Jorissen, V.V. Smith, D.L. Lambert, Astron. Astrophys. **261**, 164 (1992)
6. M. Forestini, S. Goriely, A. Jorissen et al., Astron. Astrophys. **261**, 157 (1992)
7. S. Cristallo, O. Straniero, R. Gallino et al., Astrophys. J. **696**, 797 (2009)
8. G. Meynet, M. Arnould, Astron. Astrophys. **355**, 176 (2000)
9. C. Kobayashi, N. Izutani, A.I. Karakas et al., Astrophys. J. Lett. **739**, L57 (2011)
10. M. Lugaro, C. Ugalde, A.I. Karakas et al., Astrophys. J. **615**, 934 (2004)

11. S. Palmerini, G. D'Agata, M. La Cognata et al., J. Phys: Conf. Ser. **1308**, 012016 (2019)
12. I. Indelicato, M. La Cognata, C. Spitaleri et al., Astrophys. J. **845**, 19 (2017)
13. J.J. He, I. Lombardo, D. Dell'Aquila et al., Chin. Phys. C **42**, 015001 (2018)
14. M. Wiescher, J. Gorres, H. Schatz, J. Phys. G: Nucl. Part. Phys. **25**, R133 (1999)
15. Angulo C., Arnould M., Rayet M. et al., NuPhA 656 (1999)
16. I. Lombardo, D. Dell'Aquila, A. Di Leva et al., PhLB **748**, 178 (2015)
17. M. La Cognata, A.M. Mukhamedzhanov, C. Spitaleri et al., ApJL **739**, L54 (2011)
18. G. Breuer, ZPhy **154**, 339 (1959)
19. A. Isoya, H. Ohmura, T. Momota, NuPhA **7**, 116 (1958)
20. R. Caracciolo, P. Cuzzocrea, A. De Rosa et al., Lett. Nuovo Cimento **11**, 33 (1974)
21. I. Lombardo, D. Dell'Aquila, L. Campajola et al., J. Phys. G: Nucl. Part. Phys. **40**, 125102 (2013)
22. G.L. Guardo, T. Petruse, D. Lattuada et al., EPJA **59**, 65 (2023)
23. https://www.micronsemiconductor.co.uk/
24. https://lise.nscl.msu.edu/lise.html
25. D. Lattuada, D.L. Balabanski, S. Chesnevskaya et al., EPJ Web Conf. **165**, 01034 (2017)
26. S. Chesnevskaya, D.L. Balabanski, D. Choudhury et al., JINST **13**, T05006 (2018)
27. R.J. deBoer, O. Clarkson, A. J. Couture, et al., Phys. Rev. C103, 055815 (2021)
28. L.Y. Zhang, J. Su, J.J. He et al., Phys. Rev. Lett. **127**, 152702 (2021)
29. L.Y. Zhang, J. J. He, R. deBoeur, et al., Phys. Rev. C106, 055803 (2022)
30. A. Tumino, C.A. Bertulani, M. La Cognata et al., Annu. Rev. Nucl. Part. Sci. **71**, 345–76 (2021)
31. R.G. Pizzone, G. D'Agata, M. La Cognata et al., ApJ **836**, 57 (2017)
32. G. D'Agata, R.G. Pizzone, M. La Cognata et al., ApJ **860**, 61 (2018)
33. L.Y. Zhang, J. Su, J.J. He, Wiescher, et al., Phys. Rev. Lett.,127,152702 (2021)
34. L.Y. Zhang, J. He, R.J. deBoer, et al., Nature,610, 656 (2022)
35. S. Cristallo, O. Straniero, R. Gallino et al., Astrophys. J. **696**, 797 (2009)
36. H. Jonsson, N. Ryde, E. Spitoni, E., et al., Astrophys. J, 835, 50 (2017)
37. C. Abia, K. Cunha, S. Cristallo et al., A&A **581**, A88 (2015)
38. Y.H. Kim, B. Davids, M. Williams et al., Nucl. Eng. Technol. **55**(3), 919–926 (2023)